The effect of short polystyrene brushes grafted from graphene oxide on the behavior of miscible PMMA/SAN blends

Marketa Ilcikova* [1, 2], Monika Zygo [1], Miroslav Mrlik [3], Josef Osicka [3], Milan Masar [3], Miroslav Slouf [4], Marcin Maslowski [1], Milan Kracalik [5], Robert Pietrasik [6], Jaroslav Mosnacek [2,7], Joanna Pietrasik* [1]

[1] Lodz University of Technology, Department of Chemistry, Institute of Polymer and Dye Technology, Stefanowskiego 12/16, 90 924 Lodz, Poland

[2] Polymer Institute, Slovak Academy of Sciences, Dubravska cesta 9, Bratislava 845 41, Slovakia

[3] Tomas Bata University in Zlin, University Institute, Centre of Polymer Systems, Trida T. Bati 5678, Zlin 76001, Czech Republic

[4] Institute of Macromolecular Chemistry, Czech Academy of Sciences, Heyrovskeho namesti 2, 162 06 Praha 6, Czech Republic

[5] Johannes Kepler University Linz, Institute of Polymer Sciences, Altenberger Str 69, A-4040 Linz, Austria

[6] Lodz University of Technology, Institute of Materials Science and Engineering, Stefanowskiego 1/15, 90 924 Lodz, Poland

[7] Centre for Advanced Material Application, Slovak Academy of Sciences, Dubravska cesta 9, 845 11 Bratislava, Slovakia

marketa.ilcikova@savba.sk, monika.zygo@edu.p.lodz.pl, mrlik@utb.cz, osicka@utb.cz, masar@utb.cz, slouf@imc.cas.cz, marcin.maslowski@p.lodz.pl, robert.pietrasik@p.lodz.pl, milan.kracalik@jku.at, jaroslav.mosnacek@savba.sk, joanna.pietrasik@p.lodz.pl

Corresponding authors: marketa.ilcikova@savba.sk, joanna.pietrasik@p.lodz.pl

Keywords: polymer blends, PMMA, SAN, graphene oxide, polymer brushes, SI-ATRP, rheology, nanocomposites

Abstract

A new concept of utilization of particle-polymer hybrids as multifunctional additives for polymer blends was introduced in this study. Graphene oxide particles with short densely grafted polystyrene brushes (GO-*g*-PS) were prepared by surface-initiated atom transfer radical polymerization (SI-ATRP). Melt rheology studies revealed that GO-*g*-PS suppressed the phase separation of miscible poly(methyl methacrylate)/poly(styrene-*co*-acrylonitrile) (PMMA/SAN) blends. The studies suggested specific interactions of GO-*g*-PS with the PMMA phase and this was confirmed based on calculations of activation energies of segmental relaxations by broadband dielectric spectroscopy (BDS). These unusual interactions of GO-*g*-PS with PMMA phase were assigned to the specific and precise architecture of the GO-*g*-PS particles as well as chemical nature of PS polymer brushes. The short chains of PMMA and PS provide miscibility originating from UCST behavior of PMMA/PS blend of short polymer chains. Additionally, BDS also revealed improved charge transport in PMMA/SAN blend in presence of GO-*g*-PS hybrid.

1. Introduction

Polymer blends are interesting materials since they can provide attainment of novel properties that are hardly achievable for parent homopolymers. Miscible polymer blends exhibit properties of single phase materials. They are defined as homogenous alloys down to the molecular level [1]. Nevertheless, mixing is not ideal, the level of mixing approaches the segmental scale in dimensions, and even structured morphology with several large nanometer sized domains can be observed [2].

PMMA/SAN blends are very special as they are only miscible under certain conditions. Their miscibility is affected by several factors. The acrylonitrile (AN) content in the SAN copolymer can be pointed out as the most critical parameter. The miscibility occurs only in the range of 9 to 33 wt.% of AN in SAN. Furthermore, it is affected by molar mass of the individual polymers, the ratio of PMMA and SAN in the blend, and the temperature [3]. A lower critical solution temperature (LCST) behavior can be observed in these blends. They switch from the miscible to immiscible state with increasing temperature. The transition is related to separation of polymers and formation of domains of particular compositions. The PMMA/SAN pair separate *via* the spinodal decomposition mechanism. Once the domains are large enough the blend loses specific properties, among them also transparency, thus this transition is observed as a cloud point. The properties changes are unfavorable, therefore there is a tendency to retain the materials properties in time and with increasing temperature.

The coarsening of the domains can be affected by filler addition. It has been shown, that the utilization of graphene nanoparticles resulted in formation of smaller domains compared to the neat blend [4]. The addition of sphere-like silica particles (3 wt.%) increased the decomposition

temperature (determined by melt rheology) by approximately by 10 °C for both 40/60 and 60/40 PMMA/SAN blends [5].

Recently, attention was directed to examination of particle-polymer hybrids as active functional fillers. They impart the additional material properties; such as electrical, magnetic, or mechanical reinforcement, according to particle nature, while the polymer grafts enable tailoring specific particles interactions and also their location either in the preferred phase or at the interphase of polymer blends [6].

GO-*g*-polymer hybrids were observed to significantly affect the performance of polymer blends [7-9]. In respect to miscible PMMA/SAN blends, the GO modified with PMMA chains was reported to affect morphology changes and resistivity of partially miscible PMMA/SAN upon annealing [10]. In this case the PMMA chains were long and loosely grafted (M_n 51,000 g/mol, 0.008 chains/nm^2) as the grating reaction was an uncontrolled mechanism. Modification of graphene oxide with PMMA (M_n 57,000 g/mol or 34,000 g/mol) or SAN (M_n 100,200 g/mol) was reported to enhance the LCST of PMMA/SAN blends [11, 12]. Also, in these studies the modification of the GO was performed under uncontrolled polymerization conditions resulting in very low grafting density of 0.004 chains/nm^2 [11].

The results shown above can be considered promising. However, the interactions between the polymer grafted onto particles and the host polymer are difficult to evaluate, because the polymer corona in such systems is inhomogeneous. The remaining question is whether the already reported effects could be amplified by appropriate selection of chemistry and architecture of the grafted polymer chains. It was proved that the best particle dispersion can be obtained at "optimal" grafting density [13]. While long brushes may provide entanglements with long polymer matrix chains, the low grafting density may lead to poor efficiency in interactions due to the mushroom-like

morphology of low grafting density brushes on the particle substrate. On the other hand, too densely grafted brushes provide attractive force that leads to particle flocculation and thus worse dispersion in polymer melts [13]. Thus, the optimum grafting density lies in-between these parameters, and therefore is rather difficult to reach by an uncontrolled polymerization procedure. From that point of view, the well-defined architectures of polymer grafts may provide more efficient interactions between the particles and components of the blends. The effect of well-defined polymer brushes on the physical properties of partially miscible PMMA/SAN blends has not been reported so far.

In the current study, a system based on short polymer brushes tethered on the graphene oxide particles (GO) was introduced. Polymer chains were grafted from GO surface using the SI-ATRP approach. SI-ATRP is a versatile method that allows tailoring the molecular architecture of the tethered polymer chains [14] as well as controlling the electrical conductivity of GO [15-18]. Short chains are favorable with respect to electrical conductivity of partially reduced GO as they do not significantly hinder the charge carrier movement. Thus, short polystyrene brushes were grafted from GO surface (GO-*g*-PS) and composed with poly(methyl methacrylate)/poly(styrene-*co*-acrylonitrile) (PMMA/SAN) blends. A substantial effect on the temperature stability and viscoelastic properties upon addition of a tiny amount of GO-*g*-PS was demonstrated. The origin of the favorable effect was elucidated and is ascribed to preferred interactions of the grafted polymer brushes with the PMMA polymer chains, as was revealed by broadband dielectric spectroscopy. The presented results demonstrate the importance of the well-defined architecture of polymer brushes and its significance in the design of the properties of polymer blends.

2. Experimental part

2.1. Materials

The polymer matrices poly(methyl methacrylate) (PMMA, M_w ~120,000 g/mol and $Đ$ = 2.19,)) and poly(styrene-*co*-acrylonitrile) (SAN, acrylonitrile 25 wt.%, M_w ~165,000 g/mol and $Đ$ = 2.50) were received from Aldrich and dried at 30 °C and 100 mbar overnight before processing.

Styrene (99 %), methyl 2-bromopropionate (MBP, 98 %), *N*,*N*,*N´*,*N´´*,*N´´*-pentamethyldiethylenetriamine (PMDETA, ≥99 %), copper bromide (CuBr, ≥99 %), 2-bromoisobutyryl bromide (BiBB) (98 %), triethylamine (TEA, 98 %) and anisole (99 %), diethyl ether (≥99 %) were purchased from Sigma Aldrich (USA) and used without further purification. Fuming nitric acid, potassium chlorate (KCl, p.a.), hydrochloric acid (HCl, p.a.), tetrahydrofuran (THF, p.a.), acetone (p.a.), dimethylformamide (DMF, p.a.) all were purchased from Pentalabs (CZ) and was used as received.

2.2. Methods

The molar mass (M_n) and dispersity ($Đ$) of the polymer chains were investigated by gel permeation chromatography using a GPC instrument (PL-GPC220, Agilent, Tokyo, Japan) equipped with GPC columns (Waters 515 pump, two PPS SDV 5 μm columns (diameter of 8 mm, length of 300 mm, 500 Å + 105 Å)) and a Waters 410 differential refractive index detector at 30 °C. THF was used as solvent and PS calibration was used for characterization of the molecular weight of PS.

Transmission electron microscopy (TEM) observations of unmodified GO particles and GO-*g*-PS hybrids were performed using JEM-2100Plus electron microscope (Jeol, Japan) with acceleration voltage 200 kV. The samples for the TEM analysis were prepared by dispersing the particles in acetone using mechanical stirring for 5 min followed by 2 min of sonication and dropping the resultant suspension onto a copper grid.

Transmission electron microscopy of PMMA/SAN blends and composites was performed on TEcnai G2 Spirit Twin microscope (FEI, Czech Republic). The ultrathin sections (thickness ca 60 nm) for TEM were prepared by ultramicrotomy at room temperature (ultramicrotome Ultracut UCT; Leica, Austria) and deposited on carbon coated TEM grids. The sections were stained in RuO_4 vapor for 2 h in order to increase contrast between blend components. The stained sections were observed using bright field imaging at 120 kV.

The thermal decomposition of the samples was on-line monitored using thermogravimetric analyzer (TGA) operating at 10 K/min in a nitrogen atmosphere, coupled with Fourier-transform infrared spectroscopy (FTIR) with a help of Nicolet iS10 equipped with TGA-IR module (Thermo Scientific, USA). Identification of the synthesized materials were performed by X-ray diffraction (XRD) using XRD diffractometer MiniFlex600 (Japan, RIGAKU) with Co Kα source (λ of 0.17903 nm, operating at 40 kV and 20 mA) and scan range 2θ between 5 ° and 90 °.

The surface area of samples in the form of powder was determined by using volumetric sorption analyzer, Belsorp mini-II (Microtracbel, Japan).

The pellets of GO and GO-*g*-PS were used for electrical conductivity measurements, a two–point method at room temperature was applied with the help of an electrometer (Keithley 6517B, Beaverton, OR, USA). The presented results are the average values from 10 independent measurements.

The composites consisting of the neat GO and GO modified with PS (GO-*g*-PS) and corresponding amounts of PMMA and SAN matrices were mixed using a twin-screw counter-rotating mixer provided by Brabender (Duisburg, Germany) with a volume capacity of ~50 cm^3. The instrument was heated in all heating zones at the operating temperature of 150 °C, while the feeding time was set to 1 minute followed by 5 minutes of compounding under a rotors speed of 50 rpm. The filler

concentration was 0.5 wt.%. The low polymer content in GO-*g*-PS hybrids was omitted in the calculations.

The polymer blends and their composites were characterized by melt rheology by using Physica MCR 501 rheometer (Anton-Paar, Austria). The parallel-plate geometry with plate diameter 25 mm was used in all experiments, the gap was set at 0.95 mm. The strain was set to 1 % to ensure the linear response in all measurements. The disk-shaped specimens for rheological measurements (22 mm diameter and 1.4 mm thickness) were cut from a composite sheet prepared by compression molding at 160 °C for 10 min. The samples were measured in the frequency range 0.1 to 628 rad s^{-1}, and in the temperature range from 160 to 230 °C, with 10 °C steps. Each sample was measured three times.

The dielectric measurements were performed using Broadband Dielectric Impedance Analyzer (Novocontrol Technology, Germany) equipped with standard sample cell BDCS 140. Samples in the form of a thin sheet (1 mm thick), were placed between the gold-plated electrodes (20 mm diameter). The frequency sweep was measured in the range 0.1 to 10 MHz and temperature range -150 to 150°C.

2.3. Synthesis

2.3.1. Graphene oxide and Graphene oxide modified with initiator

The synthesis of graphene oxide was performed according to a modified Brodie method [19]. The ATRP initiator bromo-2-methylpropionyl bromide (BiBB) was introduced onto the surface of the graphene oxide *via* esterification according to the literature [15]. The detailed description of both procedures can be found in SI.

2.3.2. Graphene oxide polymer hybrid

The polystyrene brushes were grafted from initiator modified graphene oxide (GO-I) under ATRP conditions. The GO-I (1 g, 0.22 mmol Br) particles were put into a Schlenk flask, which was then evacuated and backfilled with argon three times. Styrene (67.41 mL, 586.4 mmol), methyl 2-bromopropionate MBP (0.1635 mL, 1.466 mmol), *N*,*N*,*N´*,*N´´*,*N´´*-pentamethyldiethylenetriamine PMDETA (0.3061 mL, 1.466 mmol), and anisole (67 mL) were purged with argon and added into the system under argon flow. The freeze-pump-thaw cycles were performed four times, until no bubbles released from reaction mixture. The CuBr catalyst (0.2103 g, 1.466 mmol) was quickly added under argon flow into the frozen system. The molar ratio of reactants [styrene]:[MBP]:[CuBr]:[PMDETA] was [400]:[1]:[1]:[1], the solvent anisole in the amount of 50 vol.% was added. Finally, the reaction was started by the immersion of the Schlenk flask into the oil bath heated to 60 °C. The polymerization was stopped after 192 hours, at 8 % monomer conversion (determined by ^{1}H NMR). The molar mass and *Đ* of the PS chains grown from the free initiator were determined by GPC (THF, PS standard) and reached values of 3,200 g/mol and 1.09, respectively. The electrical conductivity of GO-*g*-PS hybrids reached 6.8 x 10^{-4} S cm^{-1}. The pure hybrids were separated from free PS by centrifugation followed by washing with THF. That process was repeated several times until no polymer was precipitated from the solution decanted from the hybrid particles suspension.

2.3.3. Preparation of GO-*g*-PS PMMA/SAN composites

The polymer blends were prepared by melt mixing using the Brabender internal mixer at 150 °C, 50 rpm, until constant torque was attained (10 minutes). All the components were dried (RT, 100 mbar, overnight) before blending. The concentration of GO and GO-*g*-PS was 0.5 wt.% to enable comparison with the literature data [11].

3. Results and discussion

3.1. Characterization of GO-*g*-PS hybrids

The surface area of GO was determined by BET analysis and reached 9.04 m^2 g^{-1}. The prepared GO-*g*-PS hybrids were characterized by TGA with online FTIR monitoring to prove presence of PS brushes. Three decomposition areas are visible in the TGA (see Fig. 1a). The first drop appeared in the temperature range from 25 °C to 150 °C and is attributed to evaporation of adsorbed water. At the temperature range from 150 °C to 250 °C, the decomposition of oxygen containing functional groups takes place [20, 21]. The decomposition of polymer brushes grafted from GO surface can be observed in temperature range 220 °C to 450 °C [18, 22]. Herein, the decomposition of PS brushes started at 260 °C and finished at 450 °C. At this temperature range the FTIR spectra of decomposed moieties in the form of gases were collected and analyzed (Fig. 1b). The characteristic bands of aromatic structures are clearly seen in the spectra, the C-H bond is visible at 3120 to 2880 cm^{-1}, and the C=C bond appears at 1461 cm^{-1}.

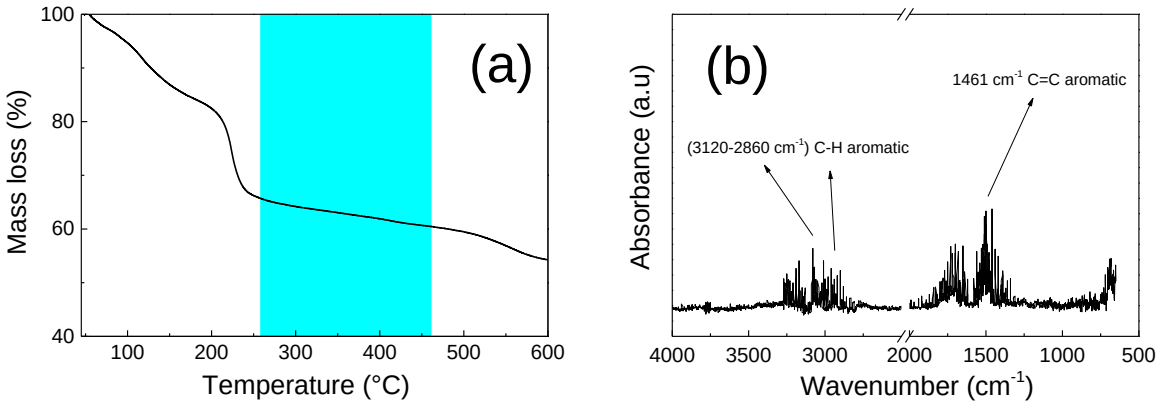

Fig. 1. Thermogravimetric analysis with FTIR online monitoring of GO-*g*-PS: (a) TGA curve, (b) FTIR spectra collected in temperature range from 260 °C to 450 °C.

The amount of decomposed organic content in temperature interval from 250 °C to 450 °C was 8 wt.%. Considering the mass loss of neat GO and GO-I (Fig. S1) in this temperature range, 5 wt.%, it can be assumed that PS chains represent 3 wt.%. Based on this information and the polymer molar mass determined by GPC, the grafting density can be estimated, assuming the similar molar mass of brushes grown from surface and sacrificial initiator [23, 24] the calculated grafting density corresponds to 0.6 chains nm^{-2} which is a relatively high value [25]. The exact formula utilized for the grafting density calculation is given in SI. The molar mass of PS brushes used in this study was 3,200 g/mol, which is a lower value than chain entanglement limit of PS, 31,200 g/mol [26], thus the dense brush regime arrangement could be expected [27]. Molar mass was not determined based on the cleaved PS from GO surface because of the low DP of the PS and low surface area of GO. As can be seen from the TGA, the GO-*g*-PS shows lower amount of oxygen functional groups compared to GO and GO-I (Fig. S1) which points to partial reduction of GO surface during SI-ATRP and it is in agreement with our previous results [15].

The presence of the PS on the GO surface was also observed by TEM. The TEM images of neat GO and GO-*g*-PS hybrids are shown in the Fig. S2a and S2b, respectively. The neat GO particles show typical 2D structure and proper exfoliation after the oxidation procedure. The darker parts can be recognized as two or three layers of individual GO sheet. The presence of the polymer shell can be seen as substantial darker tone, which covers the GO surface and also exhibits the flossy-like structure as was shown elsewhere [22, 28].

The GO modification with PS resulted in enlargement of spacing between the graphene layers, as confirmed by XRD (Fig. 2). The characteristic peak of the crystalline graphitic structure is visible at 31.2° 2Θ. After oxidation the band shifted to 17.1° 2Θ, confirming the increase of the inter-layer distance. This was further enlarged after polymerization when the 2Θ shifted to 11.8°.

According to the Bragg equation (1) the interlayer distance increased from 0.333 nm for graphite to 0.6021 nm and 0.871 nm, for GO and GO-*g*-PS, respectively.

$$n\lambda = 2d\ sin\theta \qquad (1)$$

where n is a positive integer, d is the layer distance, λ is a wavelength of incidence light and Θ is a scattering angle.

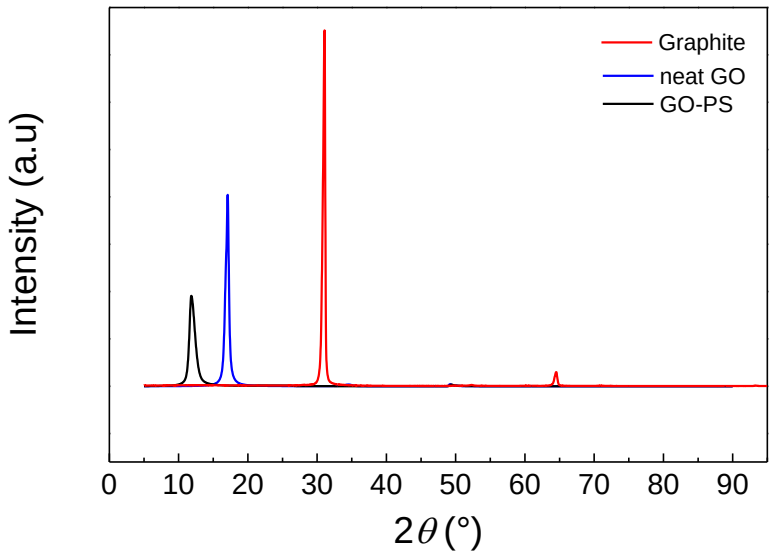

Fig. 2. XRD spectra of neat graphite, graphene oxide (GO) and polystyrene-grafted graphene oxide (GO-*g*-PS).

3.2. Characterization of neat polymer blends and composites

Polymer blends of 40/60 and 60/40 PMMA/SAN ratios were studied. Both were filled with neat GO and GO-*g*-PS polymer hybrid. The grafting of GO with PS brushes was expected to improve the particle dispersion, and also affect the polymer blend performance. The molecular weight of PS chains was targeted to approximately 3,000 g/mol. According to the literature, such value was sufficient to observe an effect on polymer blend performance [29].

3.2.1. Effect of GO and GO-*g*-PS on morphology of PMMA/SAN blends

At the LCST point the miscible blend passes through a phase transition and the morphology changes into immiscible. The PMMA/SAN pair used in this study fits the miscibility window. The miscibility was confirmed by TEM (Fig. S3), the ultrathin sections were treated with RuO_4 vapors, which would have allowed to differentiate SAN from PMMA in heterogeneous systems, as evidenced elsewhere [30]. The fine homogeneous morphology of all PMMA/SAN blends is clearly visible, similarly observed by other authors [31]. The addition of filler did not lead to phase separation, as documented by Figs. S3b, c, e, and f.

3.2.2. Effect of GO-*g*-PS on basic rheological characterization

Melt rheology is frequently used to study the flow of polymer blends, including effects related to morphological changes [32-35]. The PMMA/SAN blends were studied in frequency sweeps at 200 °C, 210 °C and 220 °C, respectively. The temperature 230 °C is a ceiling temperature for PMMA, above it depolymerization followed by gelation would occur, especially in the presence of moisture [33, 36]. Cross-linked structures are formed, and they provide long relaxation times. They appear in frequency dependence of G' as a flattening of the slope at low frequencies. In this region morphological changes are observed as well. Therefore, the rheological studies were also conducted below this temperature. In the Fig. 3 the dependence of complex viscosity (η^*) against angular frequency (ω) of polymer blends and their composites is depicted in logarithmic scales.

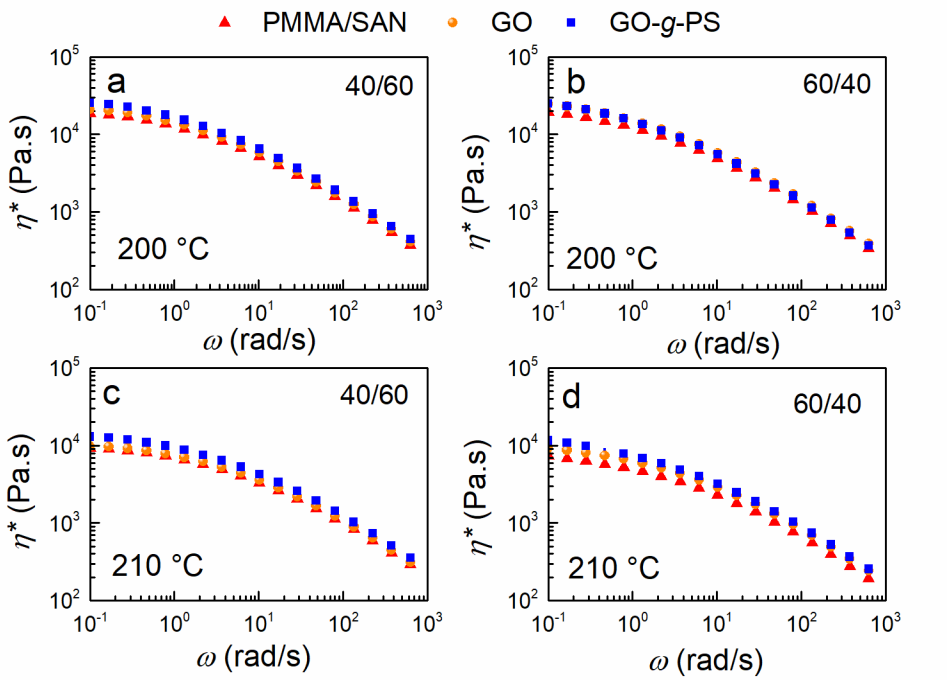

Fig. 3. The angular frequency dependence of complex viscosity of PMMA/SAN 40/60 and 60/40 matrices, composites containing 0.5 wt.% GO and GO-*g*-PS. The data collected at 200 °C (a, b), 210 °C (c, d).

At 200 °C, the effect of surface modification can be seen in Fig. 3 a, b, however it is more pronounced at 210 °C (Fig. 3 c, d). When compared the values of η^* within the plateau region (0.1 Hz) at 210 °C the η^* of 40/60 PMMA/SAN increased by 6 % and 41 % after addition of neat GO and GO-*g*-PS, respectively (Fig. 3c). However, the most noticeable improvement of η^* within the same range of frequency is visible in the 60/40 system at 210 °C where the η^* of 60/40 PMMA/SAN increased by 26 % and 58 % after addition of neat GO and GO-*g*-PS, respectively (Fig. 3d). The effect of GO can be assigned to steric hindrance, while in the case of GO-*g*-PS the specific interactions between components of PMMA/SAN blend and PS grafts present on the surface of GO probably contribute in the increase of η^*, as is discussed further. The effect is also

visible from *G'(ω)* dependence, Fig. 4. The temperature of 220 °C was selected because the observed changes were the most significant under these conditions.

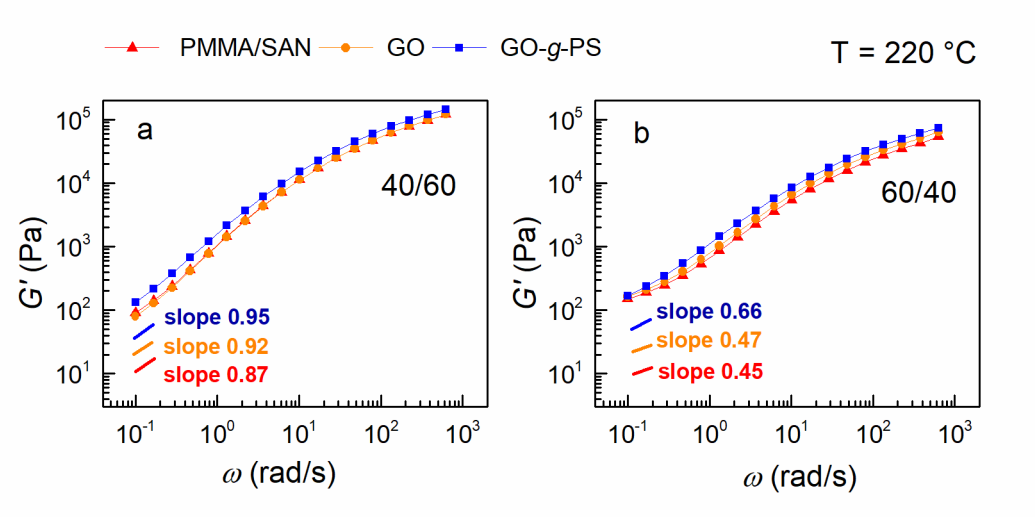

Fig. 4. The angular frequency dependence of storage modulus (*G'*) of PMMA/SAN 40/60 (a) and PMMA/SAN 60/40 (b) blends, and composites containing 0.5 wt.% GO and GO-*g*-PS. The data collected at 220 °C.

The dependence shows an arc-like shape typical for homopolymers, the rubbery plateau followed by the decrease of *G'* with decreasing frequency. Slight narrowing of the slope at low frequencies can be observed. It indicates the presence of phase-separated domains. In both 40/60 and 60/40 systems the composites with GO-*g*-PS provide the highest slope at low frequencies, while the effect is more pronounced in the 60/40 system which proves that presence of GO-*g*-PS suppress the phase separation.

3.3.3. Morphology effects studied by rheological measurement

The LCST transition of polymer blends can be studied using dynamic shear rheology. The transition appears as a drift from semicircle in Cole-Cole plot [33]. The Cole-Cole plot represents

the dependence of imaginary part of $\eta^*(\eta'')$ versus real part of $\eta^*(\eta')$ (where $\eta'' = G'/\omega$ and $\eta' = G''/\omega$, *and G' and G''* represent the real and imaginary parts of the shear complex storage modulus, respectively) . Below LCST, in homogeneous state, there is only one circular arc in the plot. Above LCST, a tail or a second circular arc appears on the right-hand side of the arc, which indicates a second relaxation mechanism and denotes a formation of second phase [33, 37]. It should be also noted that the arc become smaller and located in left bottom corner as the material softens. For better understanding the evolution of the Cole-Cole an example of dependence of PMMA/SAN 40/60 sample with temperature is depicted in Fig. S4.

The Cole-Cole plots of 40/60 and 60/40 blends and their composites are shown in Fig. 5. In the 40/60 blend system, the formation of the second arc related to phase separation starts at 220 °C in both neat matrix and composite (Fig. 5c). On the other hand, in the 60/40 blend system, the phase separation begins to occur at around 210 °C (Fig. 5b), the second arc is clearly formed in the neat blend as well as the GO composite, while in GO-*g*-PS composite the flattening of the curve can be seen, but not the tail of the second arc yet. The PS brushes suppress the second arc formation in this case. The tail of second peak clearly appeared at 220 °C. The precise determination of LCST was not possible from the obtained data sets due to the fact that the measurements were performed with 10 °C steps. But the results clearly show the effect of GO-*g*-PS on the LCST and are more efficient in 60/40 blend composition. A similar observation was reported for PMMA/SAN blend stabilized with silica nanoparticles grafted with PS brushes (silica-*g*-PS) [5]. The silica particles were grafted with short (500 g/mol or 2,000 g/mol) chains and long (46,000 g/mol) that fully screened the particle core. Regardless of preferred interactions and particle location upon annealing, the enhancement of LCST was observed for all types of modified silica. A comparison with the literature data suggests the GO-*g*-PS hybrids are more efficient then silica-*g*-PS particles.

The incorporation of 3 wt. % of silica-*g*-PS into the 40/60 PMMA/SAN blend resulted in enhancement of LCST by 2 °C, from approx.174 °C to 176 °C, and in the 60/40 PMMA/SAN blend by approx. 10 °C, from 166 °C to 176 °C [5]. Herein, the enhancement of LCST for both PMMA/SAN ratios was in the similar range, i.e. up to 10 °C but it was achieved by adding only 0.5 wt. % of GO-*g*-PS hybrids, Fig. 5.

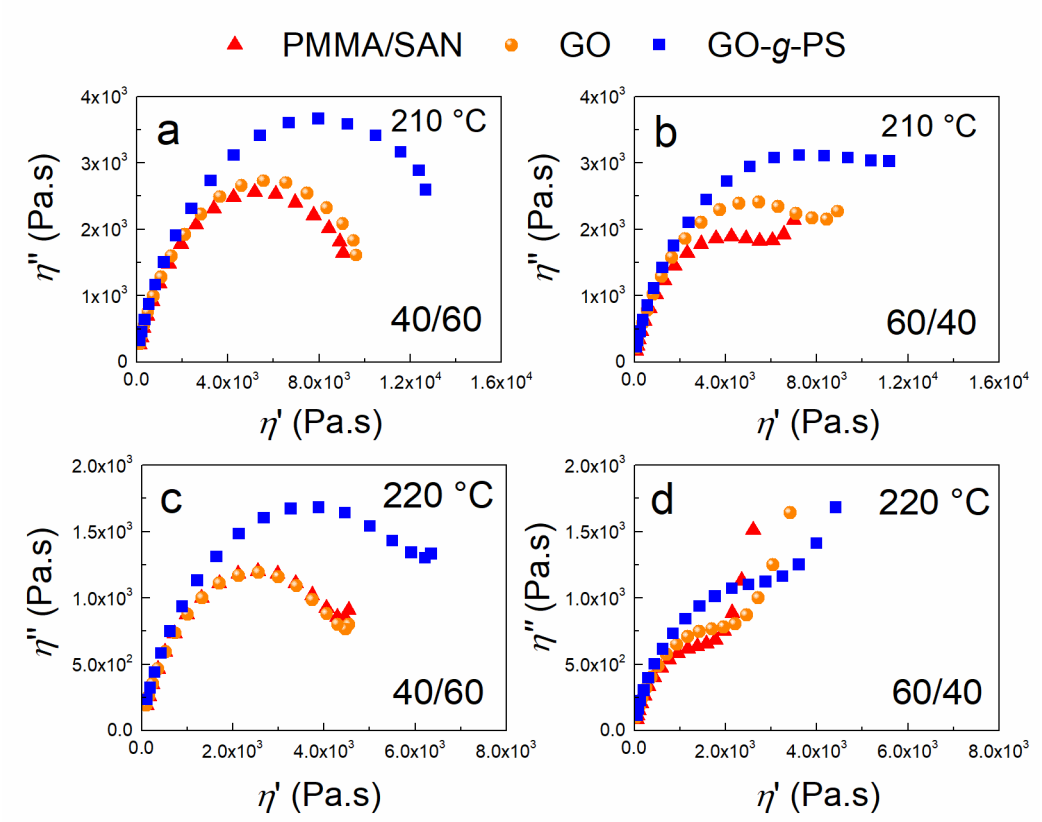

Fig. 5. The Cole-Cole plots of PMMA/SAN 40/60 and 60/40 blends, composites containing 0.5 wt.% GO and GO-*g*-PS. The data collected at 210 °C (a, b) and 220 °C (c, d).

To provide quantitative comparison of the effectivity of the filler on the blend temperature stabilization, the data were fitted by Cole-Cole model (2) [38]. The fitting of the main arc was performed for 200 °C and 210 °C.

$$\eta^* = \eta_\infty + (\eta_0 - \eta_\infty) \times \frac{1}{[1 + (i\omega\tau)^\alpha]} \quad (2)$$

where η^* is the complex viscosity, η_∞ is the unrelaxed viscosity, η_0 is the relaxed viscosity, i is the characteristic complex number, ω is the angular frequency (where $\omega = 2\pi f$), τ is the relaxation time and α is shape characteristic of the fitted curve where $0 < \alpha$.

The data fitted with the model are shown in Fig. S5. In Table 1, the parameters $\Delta\eta$, that correspond to $\eta_0 - \eta_\infty$, and relaxation times τ of the fit functions are summarized.

Table 1 Parameters of Cole-Cole model.

	40/60 PMMA/SAN, 200 °C			**60/40 PMMA/SAN, 200 °C**		
	matrix	**GO 0.5 wt. %**	**GO-*g*-PS 0.5 wt. %**	**matrix**	**GO 0.5 wt. %**	**GO-*g*-PS 0.5 wt. %**
$\Delta\eta$ (Pa.s)	22190	25100	31570	22560	28930	34190
τ (s)	0.151	0.181	0.247	0.202	0.242	0.390
a	0.600	0.599	0.591	0.583	0.580	0.5416

	40/60 PMMA/SAN, 210 °C			**60/40 PMMA/SAN, 210 °C**		
	matrix	**GO 0.5 wt. %**	**GO-*g*-PS 0.5 wt. %**	**matrix**	**GO 0.5 wt. %**	**GO-*g*-PS 0.5 wt. %**
$\Delta\eta$ (Pa.s)	8340	9870	11950	8410	10730	13970
τ (s)	0.083	0.089	0.141	0.106	0.113	0.205)
a	0.598	0.586	0.581	0.557	0.551	0.545

The value of τ reflects the polymer chain mobility. The addition of neat GO resulted in slight increase of τ compared to neat matrix at both investigated temperatures, 200 °C and 210 °C which points to a slight restriction of polymer chains of the polymer blend matrix in presence of GO. On the other hand, the addition of 0.5 wt. % of GO-*g*-PS changed τ of both 40/60 and 60/40 matrices. At 200 °C the relaxation time of 40/60 PMMA/SAN blend increased from 0.151 s to 0.247 s, that is an increase by 64 %, and τ reported in 60/40 PMMA/SAN blend was changed by 93 %. At 210 °C the τ increased from 0.083 to 0.141 s, i.e. by 70 % in 40/60 blend and by 93 % at 60/40 blend. Similar trends are observed in $\Delta\eta$, which reflects the enhancement of viscosity. The more pronounced effects of GO-*g*-PS appeared in 60/40 PMMA/SAN blend. The results obtained from melt rheology suggest specific interactions of GO-*g*-PS with PMMA/SAN blend.

3.3.4. Elucidation of specific interactions of the filler and PMMA/SAN matrix

In order to attain a better understand the obtained results, we further focused on elucidation of interactions of the GO-*g*-PS particles with individual components of the PMMA/SAN blend.

Theoretical prediction of GO-*g*-PS particle location above LCST in PMMA/PS blend was based on the wetting parameter ω, calculated from equation (3):

$$\omega = \frac{\gamma_{S-2} - \gamma_{S-1}}{\gamma_{12}} \quad (3)$$

where γ_{S-1}, γ_{S-2} and γ_{12} is interfacial tension between the filler and polymer 1, the filler and polymer 2 and the two polymers 1 and 2, respectively. If $\omega > 1$, the filler is mainly distributed in polymer 1; if $\omega < -1$, the filler is situated in polymer 2, and if $-1 < \omega < 1$, the particles are located at the interface between polymer 1 and polymer 2 [39].

The calculation of the wetting coefficient (Table S1) are based on values of the interfacial tensions, adopted from literature, points to not-preferred interactions of GO-*g*-PS, either with PMMA or SAN. This could suggest that the preferential particles location is at the interphase above LCST. However, it should be mentioned that the calculations did not take into account the change of polymer polarity with the temperature and the impact of molecular weight of polymers on the surface tension. On the other hand, the miscibility of PMMA/PS blend was reported in a case of linear polymers as well as polymer brushes systems [40-42]. Although the Flory-Huggins interaction parameter reveals a strong repulsive interaction between PMMA and PS, miscibility was observed for polymers with low molar masses above the UCST transition [43]. The blend of silica particles grafted with PS brushes (6,500 g/mol, 0.76 chains/nm^2) and PMMA brushes (6,800 g/mol, 0. 41 chains/nm^2), respectively, both in the dense brush regime, were found to be miscible. Such hybrids turned immiscible upon crossing a certain molar mass threshold [42]. The reason of such behavior was assigned to the reduced segmental interactions of chemically different chains due to dense brush arrangement, and presence of particles cores that decrease the segmental contacts that would drive the phase separation.

The GO-*g*-PS hybrids exhibited similar features and full screening of the graphene oxide can be expected due to high grafting density of tethered brushes. Thus, the interactions of PS chains with PMMA phase could be expected. As was revealed by GPC measurements, the PMMA matrix have broad distribution of molar mass, $Đ$ = 2.19, therefore, the presence of sufficiently high content of short chains fraction that could provide the partial interdigitation with PS brushes could be expected.

The interaction of GO-*g*-PS with PMMA/SAN and higher efficiency in 60/40 system could then be ascribed to the combination of the effect of brushes chemistry and their uniform architecture as well as the effect of particle core alone.

3.3.5. Specific interactions studied by dielectric spectroscopy

The specific interactions of the GO-*g*-PS with PMMA phase of PMMA/SAN blends were further confirmed by the dielectric relaxation spectroscopy. Dielectric spectroscopy enables the study of polymer chain dynamics in a broad frequency and temperature range and enables the study of the interactions of particles with the polymer matrix through effects on relaxations. The relaxations of the polymer backbones (α), side groups (β, γ) and charge mobility at the interface (interfacial polarization or Maxwell-Wagner-Sillars (MWS)) can be identified and effects of the various types of fillers on the mentioned processes can be specified [2, 44-46].

The detailed analysis of dielectric maps of neat PMMA and SAN components as well as analysis of 40/60 and 60/40 polymer blends is shown in Fig. S6a, b, S7 and S8, respectively. To evaluate the effects of the filler on the relaxation processes qualitatively, the activation energies (E_a) of the transitions were calculated. The relaxation processes and their fits are shown in Fig. 6.

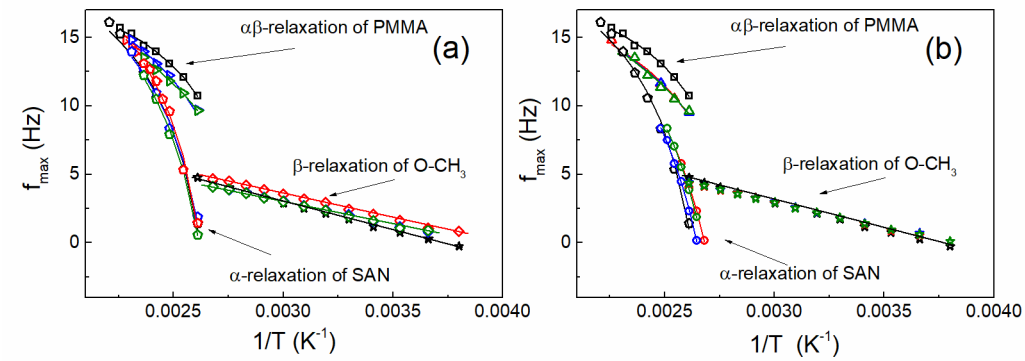

Fig. 6. Dielectric relaxation maps for VFT and Arrhenius types of relaxations, where (a) are 40/60 and (b) are 60/40 PMMA/SAN-based blends: (red) PMMA/SAN, (blue) PMMA/SAN with GO,

(green) PMMA/SAN with GO-*g*-PS. Black squares correspond to $\alpha\beta$-relaxation of pure PMMA, black pentagons correspond to α-relaxation of pure SAN and black stars correspond to β-relaxation of O-CH_3 side groups from pure PMMA. In (a) right triangles correspond to $\alpha\beta$-relaxation of PMMA in blends, diamonds correspond to β relaxation in PMMA in blends, colored pentagons correspond to α-relaxation of SAN in blends. In (b) triangles correspond to $\alpha\beta$-relaxation of PMMA in blends, stars correspond to β-relaxation in PMMA in blends, circles correspond to α-relaxation of SAN in blends.

Fig. 6 omitted the γ relaxation since it followed linear temperature dependence of frequency peak maxima. Therefore, the data were fitted with Arrhenius model (4), which allowed the calculation of the E_a transition.

$$f_\beta = f_0 \exp\left(\frac{E_a}{k_B T}\right) \quad (4)$$

where E_a is the activation energy, f_0 is the pre-exponential factor, T is thermodynamic temperature, and k_B is Boltzmann constant.

The results are listed in Table S2. The addition of either GO or GO-*g*-PS provides only negligible changes of E_a in the both the 40/60 as well as 60/40 PMMA/SAN blends. Similarly, as can be seen in Table 2, a negligible effect was observed for the β relaxation of PMMA studied in temperature range from 0 °C to 100 °C. The α relaxations corresponds to micro-Brownian motion of the main chain appeared at temperatures above T_g, in the range from 110 °C to 150 °C. In case of PMMA the cooperative $\alpha\beta$ relaxation was studied, due to the fact, that presence of neat α relaxation was above the Tg and is hardly distinguishable, as was already discussed (SI). In both blend

components, PMMA and SAN, the temperature dependence of f_{max} was non-linear and therefore data were fitted with empirical Vogel-Fulcher-Tamman equation (VFT) equation 5.

$$f = f_0 \exp\left(\frac{E_a}{R(T - T_0)}\right) \quad (5)$$

where f is the relaxation frequency, f_0 is the pre-exponential factor, E_a is the activation energy, T is the thermodynamic temperature, T_0 is Vogel temperature, and k is the Boltzmann's constant. The all fit parameters are listed in Table S3. The α relaxation of SAN showed very small changes in values of E_a after addition of filler, up to approximately 3 %, Table 2.

Table 2 Parameters of VFT fits of PMMA $\alpha\beta$ relaxation and SAN α relaxations, and Arrhenius fit of PMMA β relaxation

	E_a (kJ mol^{-1})			
	VFT $\alpha\beta$ **relaxation PMMA**	**VFT** α **relaxation SAN**	**Arhenius** β **relaxation PMMA**	**VFT MWS**
PMMA/SAN 40/60	65.6	63.0	27.7	35.6
PMMA/SAN 40/60 GO	68.9	63.9	28.6	36.4
PMMA/SAN 40/60 GO-*g*-PS	72.1	65.1	28.7	34.4
PMMA/SAN 60/40	66.3	64.2	29.9	35.0
PMMA/SAN 60/40 GO	75.2	65.5	30.3	35.1
PMMA/SAN 60/40 GO-*g*-PS	82.7	66.3	30.4	31.3

Such an increase may indicate rather limited specific interaction of GO-*g*-PS with SAN chains. In the case of PMMA $\alpha\beta$ relaxation, the blend 40/60 exhibited values of activation energy of 65.6 kJ mol^{-1}, while the blends with neat GO and GO-*g*-PS showed values of 68.9 and 72.1 kJ mol^{-1}, respectively. This corresponds to an increase by 5 % and 10 % in case of GO and GO-*g*-PS, respectively. Such changes of E_a indicate the more difficult PMMA backbone movement and thus a reinforcing effect of the filler. In the 60/40 blend the effect is even more pronounced. The E_a increased from 66.3 kJ mol^{-1} for the neat blend to 75.2 and 82.7 kJ mol^{-1} for neat blend with GO and GO-*g*-PS, respectively, an increase of 14 % and 25 %. These results prove the presence of favored interactions between GO-*g*-PS and the PMMA component of the blend. In addition, the MWS polarization was significantly affected by the presence of GO-*g*-PS. As can be seen in Table 2, the values of activation energy decreased compared to neat blends in both 40/60 and 60/40 systems, indicating the decreased charge accumulation on the interface and thus energetically easier electron mobility through the material, that results in the considerable enhancement of electrical conductivity of the investigated samples. These findings were also confirmed by decreasing relaxation time since the response to the applied electric field is due to the enhanced mobility on the interface. The presence of GO-*g*-PS facilitates the movement of the charge carries over the interface, that is related to improved electrical conductivity of the composite systems, as was proved in Fig. S9. For instance, in the 40/60 blend system the σ of the blends was changed nearly by 1.5-fold, from $5x10^{-14}$ to $2x\ 10^{-12}$ S/cm. Regarding the possible conductivity improvement it should be also stated here that the filler (GO-*g*-PS) used in this study has conductivity only in order of 10^{-4} S cm^{-1}, while utilizing the SI-ATRP approach for GO modification it was possible to reach the conductivity of the hybrid particles in the single-step in order of 10^{0} S cm^{-1} [15]. Thus, it can be assumed that the percolation of the conductivity can be

achieved at even lower filler content. Although the absolute values of electrical conductivity are low in the systems studied here (hybrid content 0.5 wt. %), this knowledge is beneficial for design of novel conductive polymer blend composites.

4. Conclusion

The effect of GO-*g*-PS hybrid grafted with short dense brushes on temperature dependent viscoelastic properties and molecular chain dynamic of miscible PMMA/SAN blends was investigated. Taking advantage of the miscibility of short PS and PMMA chains, the utilization of very small amounts of GO-*g*-PS hybrids led to an increase of the LCST, especially in a PMMA/SAN 60/40 blend system. Both techniques, melt rheology and dielectric spectroscopy, confirmed the preferred interactions of GO-*g*-PS hybrid with the PMMA matrix component. Although the dense brushes do not provide chain entanglements with polymer matrix components, they significantly improve the thermal stability of the blend as a consequence of modification of the nature of the polymer surface, including both van der Waals interactions and depletion effect. Additionally, the presence of semi-conductive hybrid particles GO-*g*-PS proved to facilitate the charge transport at the interphase without the necessity of any annealing. Although the enhancement of LCST in the presence of GO-*g*-PS is only in the order of several degrees, when considering the time-temperature superposition principle, the stabilization of miscible PMMA/SAN with only 0.5 wt. % of GO-*g*-PS hybrids can be significant in prolonging service time. The results point out that the GO-*g*-polymer hybrids with short dense brushes are a promising new type of multifunctional additives for polymer blends. Such knowledge is beneficial and provides new perspectives for the future of materials design, including miscible PMMA/SAN blends composites.

Acknowledgement

The authors thank to Action Austria – Slovakia, Co-operation in Science and Education program, project Nr. 56337 as well as to National Science Centre, Poland for the financial support through POLONEZ project number UMO-2016/23/P/ST5/02131. This project is carried out under POLONEZ program which has received funding from the European Unions' Horizon 2020 research and innovation program under Marie Sklodowska-Curie grant agreement. No 665778. This study was also performed during the implementation of the project Building-up Centre for advanced materials application of the Slovak Academy of Sciences, ITMS project code 313021T081 supported by Research & Innovation Operational Programme funded by the ERDF. JM acknowledge for financial support to project VEGA 2/0129/19. Electron microscopy at the Institute of Macromolecular Chemistry was supported by project TN01000008 (Technology Agency of the CR). This work was supported by the Ministry of Education, Youth and Sports of the Czech Republic - DKRVO (RP/CPS/2020/003).

Conflicts of interest There are no conflicts to declare.

Authors contribution

Marketa Ilcikova: Conceptualization, Methodology, Formal Analysis, Writing-original draft preparation. Monika Zygo: Formal analysis. Miroslav Mrlik: Formal analysis, Investigation. Josef Osicka: Investigation. Milan Masar: Investigation. Miroslav Slouf: Investigation. Marcin Maslowski: Resources. Milan Kracalik: Resources. Robert Pietrasik: Resources. Jaroslav

Mosnacek: Supervision, Writing-Original draft preparation. Joanna Pietrasik: Supervision, Writing-Original draft preparation.

Graphical abstract

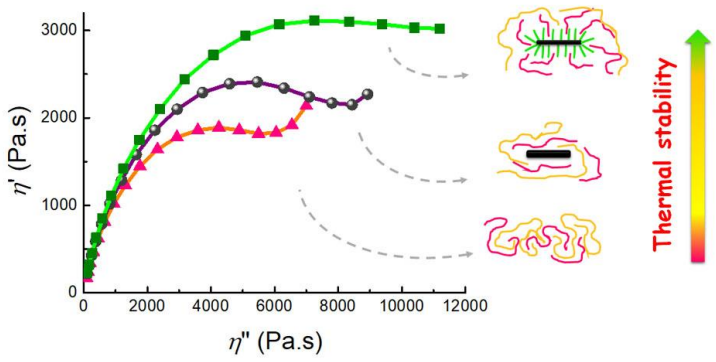

Literature

[1] L.A. Utracki, Compatibilization of polymer blends, Can. J. Chem. Eng. 80(6) (2002) 1008-1016.

[2] L.M. Robeson, Polymer Blends A Comprehensive Review, Hanser Publishers, Munich, 2007.

[3] M. Suess, J. Kressler, H.W. Kammer, The miscibility window of poly(methylmethacrylate)/poly(styrene-co-acrylonitrile) blends, Polymer 28(6) (1987) 957-960.

[4] Y.M. Kou, X. Cheng, C.W. Macosko, Polymer/Graphene Composites via Spinodal Decomposition of Miscible Polymer Blends, Macromolecules 52(20) (2019) 7625-7637.

[5] C. Huang, J. Gao, W. Yu, C. Zhou, Phase Separation of Poly(methyl methacrylate)/Poly(styrene-co-acrylonitrile) Blends with Controlled Distribution of Silica Nanoparticles, Macromolecules 45(20) (2012) 8420-8429.

[6] M. Zygo, M. Lipinska, Z. Lu, M. Ilcíková, M.R. Bockstaller, J. Mosnacek, J. Pietrasik, New type of montmorillonite compatibilizers and their influence on viscoelastic properties of ethylene propylene diene and methyl vinyl silicone rubbers blends, Applied Clay Science 183 (2019) 105359.

[7] W.H. Ferreira, C.A. Silva, C.T. Andrade, Improved compatibilization and shape memory properties of poly (3-hydroxybutyrate-co-3-hydroxyvalerate)/poly(ethylene-co-vinyl acetate) blends by incorporation of modified reduced graphene oxide, Polymer 201 (2020).

[8] Y.W. Cao, J.C. Feng, P.Y. Wu, Polypropylene-grafted graphene oxide sheets as multifunctional compatibilizers for polyolefin-based polymer blends, Journal of Materials Chemistry 22(30) (2012) 14997-15005.

[9] Y.Q. Tan, L.J. Fang, J.L. Xiao, Y.H. Song, Q. Zheng, Grafting of copolymers onto graphene by miniemulsion polymerization for conductive polymer composites: improved electrical conductivity and compatibility induced by interfacial distribution of graphene, Polymer Chemistry 4(10) (2013) 2939-2944.

[10] J.F. Zhang, M. Zuo, X. Lv, H.M. Zhang, Q. Zheng, Effect of grafted graphene nanosheets on morphology evolution and conductive behavior of poly(methyl methacrylate)/poly(styrene-co-acrylonitrile) blends during isothermal annealing, Rsc Advances 8(26) (2018) 14579-14588.

[11] T.S. Muzata, P.L. Jagadeshvaran, G.P. Kar, S. Bose, Phase miscibility and dynamic heterogeneity in PMMA/SAN blends through solvent free reactive grafting of SAN on graphene oxide, Phys. Chem. Chem. Phys. 20(29) (2018) 19470-19485.

[12] T.S. Muzata, S. Bose, Polymer tethered graphene oxide influences miscibility and cooperative relaxation in LCST blends, Polymer 188 (2020) 13.

[13] R. Hasegawa, Y. Aoki, M. Doi, Optimum graft density for dispersing particles in polymer melts, Macromolecules 29(20) (1996) 6656-6662.

[14] C.M. Hui, J. Pietrasik, M. Schmitt, C. Mahoney, J. Choi, M.R. Bockstaller, K. Matyjaszewski, Surface-Initiated Polymerization as an Enabling Tool for Multifunctional (Nano-)Engineered Hybrid Materials, Chemistry of Materials 26(1) (2014) 745-762.

[15] M. Ilcikova, M. Mrlik, Z. Spitalsky, M. Micusik, K. Csomorova, V. Sasinkova, A. Kleinova, J. Mosnacek, A tertiary amine in two competitive processes: reduction of graphene oxide vs. catalysis of atom transfer radical polymerization, Rsc Advances 5(5) (2015) 3370-3376.

[16] M. Mrlik, M. Cvek, J. Osicka, R. Moucka, M. Sedlacik, V. Pavlinek, Surface-initiated atom transfer radical polymerization from graphene oxide: A way towards fine tuning of electric conductivity and electro-responsive capabilities, Materials Letters 211 (2018) 138-141.

[17] E. Kutalkova, M. Mrlik, M. Ilcikova, J. Osicka, M. Sedlacik, J. Mosnacek, Enhanced and Tunable Electrorheological Capability using Surface Initiated Atom Transfer Radical Polymerization Modification with Simultaneous Reduction of the Graphene Oxide by Silyl-Based Polymer Grafting, Nanomaterials 9(2) (2019).

[18] M. Mrlik, M. Ilcikova, T. Plachy, V. Pavlinek, Z. Spitalsky, J. Mosnacek, Graphene oxide reduction during surface-initiated atom transfer radical polymerization of glycidyl methacrylate: Controlling electro-responsive properties, Chemical Engineering Journal 283 (2016) 717-720.

[19] O. Jankovsky, P. Marvan, M. Novacek, J. Luxa, V. Mazanek, K. Klimova, D. Sedmidubsky, Z. Sofer, Synthesis procedure and type of graphite oxide strongly influence resulting graphene properties, Applied Materials Today 4 (2016) 45-53.

[20] W. Cai, R.D. Piner, F.J. Stadermann, S. Park, M.A. Shaibat, Y. Ishii, D. Yang, A. Velamakanni, S.J. An, M. Stoller, J. An, D. Chen, R.S. Ruoff, Synthesis and Solid-State NMR

Structural Characterization of 13C-Labeled Graphite Oxide, Science 321(5897) (2008) 1815-1817.

[21] E. Aliyev, V. Filiz, M.M. Khan, Y.J. Lee, C. Abetz, V. Abetz, Structural Characterization of Graphene Oxide: Surface Functional Groups and Fractionated Oxidative Debris, Nanomaterials 9(8) (2019).

[22] J. Osicka, M. Ilcikova, M. Mrlik, A. Minarik, V. Pavlinek, J. Mosnacek, The Impact of Polymer Grafting from a Graphene Oxide Surface on Its Compatibility with a PDMS Matrix and the Light-Induced Actuation of the Composites, Polymers 9(7) (2017) 14.

[23] C. Kang, R. Crockett, N.D. Spencer, The influence of surface grafting on the growth rate of polymer chains, Polymer Chemistry 7(2) (2016) 302-309.

[24] K. Ohno, T. Morinaga, K. Koh, Y. Tsujii, T. Fukuda, Synthesis of monodisperse silica particles coated with well-defined, high-density polymer brushes by surface-initiated atom transfer radical polymerization, Macromolecules 38(6) (2005) 2137-2142.

[25] Y. Tsujii, K. Ohno, S. Yamamoto, A. Goto, T. Fukuda, Structure and properties of high-density polymer brushes prepared by surface-initiated living radical polymerization, in: R. Jordan (Ed.), Surface-Initiated Polymerization I2006, pp. 1-45.

[26] J. Hepperle, H. Munstedt, P.K. Haug, C.D. Eisenbach, Rheological properties of branched polystyrenes: linear viscoelastic behavior, Rheologica Acta 45(2) (2005) 151-163.

[27] J. Choi, C.M. Hui, J. Pietrasik, H.C. Dong, K. Matyjaszewski, M.R. Bockstaller, Toughening fragile matter: mechanical properties of particle solids assembled from polymer-grafted hybrid particles synthesized by ATRP, Soft Matter 8(15) (2012) 4072-4082.

[28] J. Osicka, M. Mrlik, M. Ilcikova, L. Munster, P. Bazant, Z. Spitalsky, J. Mosnacek, Light-Induced Actuation of Poly(dimethylsiloxane) Filled with Graphene Oxide Grafted with Poly(2-(trimethylsilyloxy)ethyl Methacrylate), Polymers 10(10) (2018) 12.

[29] Z.J. Huang, L. Li, X.A. Zhang, N. Alsharif, X.J. Wu, Z.W. Peng, X.Y. Cheng, P. Wang, K.A. Brown, Y.H. Wang, Photoactuated Pens for Molecular Printing, Advanced Materials 30(8) (2018) Article Number: 1705303.

[30] J. Rybnicek, R. Lach, W. Grellmann, M. Lapcikova, M. Slouf, Z. Krulis, E. Anisimov, J. Hajek, Ternary PC/ABS/PMMA blends - morphology and mechanical properties under quasi-static loading conditions, Polimery 57(2) (2012) 87-94.

[31] L.C. Costa, A.T. Neto, E. Hage, PMMA/SAN and SAN/PBT nanoblends obtained by blending extrusion using thermodynamics and microrheology basis, Express Polym. Lett. 8(3) (2014) 164-176.

[32] Q. Zheng, M. Du, B.B. Yang, G. Wu, Relationship between dynamic theological behavior and phase separation of poly(methyl methacrylate)/poly(styrene-co-acrylonitrile) blends, Polymer 42(13) (2001) 5743-5747.

[33] D. Chopra, M. Kontopoulou, D. Vlassopoulos, S.G. Hatzikiriakos, Effect of maleic anhydride content on the rheology and phase behavior of poly(styrene-co-maleic anhydride)/poly(methyl methacrylate) blends, Rheologica Acta 41(1-2) (2002) 10-24.

[34] Y.J. Kim, G.S. Shin, I.T. Lee, B.K. Kim, Miscible and immiscible blends of ABS with PMMA. 1. Morphology and rheology, J. Appl. Polym. Sci. 47(2) (1993) 295-304.

[35] J.S. Reinaldo, L.M. Pereira, E.D. Silva, M.M. Ueki, E.N. Ito, Effect of the chemical structure on the linear viscoelastic behavior of acrylic and styrenic polymer blends, Polymer Testing 67 (2018) 257-265.

[36] J.L. Osborne, G.C. Sarti, W.J. Koros, H.B. Hopfenberg, Zero migration of monomers in glassy polymers-a possible artifact of thermal depolymerization, Polym. Eng. Sci. 23(9) (1983) 473-488.

[37] R.M. Li, W. Yu, C.X. Zhou, Phase behavior and its viscoelastic responses of poly(methyl methacrylate) and poly(styrene-co-maleic anhydride) blend systems, Polymer Bulletin 56(4-5) (2006) 455-466.

[38] C.A. Garcia-Franco, D.W. Mead, Rheological and molecular characterization of linear backbone flexible polymers with the Cole-Cole model relaxation spectrum, Rheologica Acta 38(1) (1999) 34-47.

[39] M. Sumita, K. Sakata, S. Asai, K. Miyasaka, H. Nakagawa, Dispersion of fillers and the electrical conductivity of polymer blends filled with carbon black, Polymer Bulletin 25(2) (1991) 265-271.

[40] L.M. Dong, D.J.T. Hill, Y.P. Cai, J.W. Zheng, Miscibility in blends of polystyrene and poly(methyl methacrylate) studied by nonradiative energy transfer, Polymer Bulletin 32(3) (1994) 347-352.

[41] C.M. Burns, W.N. Kim, Solution blendig of polystyrene and poly(methyl methacrylate), Polym. Eng. Sci. 28(21) (1988) 1362-1372.

[42] M. Schmitt, J.N. Zhang, J. Lee, B. Lee, X. Ning, R. Zhang, A. Karim, R.F. Davis, K. Matyjaszewski, M.R. Bockstaller, Polymer ligand-induced autonomous sorting and reversible phase separation in binary particle blends, Sci. Adv. 2(12) (2016) 10.

[43] T.P. Russell, R.P. Hjelm, P.A. Seeger, Temperature dependence of the interaction parameter of polystyrene and poly(methyl methacrylate), Macromolecules 23(3) (1990) 890-893.

[44] H.Y.a.A.S. nhals, Broadband Dielectric Spectroscopy on Polymer Blends, Springer Science+Business Media, Dordrecht, 2014.

[45] J. Osicka, M. Mrlik, M. Ilcikova, B. Hanulikova, P. Urbanek, M. Sedlacik, J. Mosnacek, Reversible Actuation Ability upon Light Stimulation of the Smart Systems with Controllably Grafted Graphene Oxide with Poly (Glycidyl Methacrylate) and PDMS Elastomer: Effect of Compatibility and Graphene Oxide Reduction on the Photo-Actuation Performance, Polymers 10(8) (2018) 14.

[46] H. Valentova, M. Ilcikova, K. Czanikova, Z. Spitalsky, M. Slouf, J. Nedbal, M. Omastova, Dynamic Mechanical and Dielectric Properties of Ethylene Vinyl Acetate/Carbon Nanotube Composites, J. Macromol. Sci. Part B-Phys. 53(3) (2014) 496-512.

Supporting Information

The effect of short dense polystyrene brushes grafted from graphene oxide on the behavior of miscible PMMA/SAN blends

Marketa Ilcikova* [1, 2], Monika Zygo [1], Miroslav Mrlik [3], Josef Osicka [3], Milan Masar [3], Miroslav Slouf [4], Marcin Maslowski [1], Milan Kracalik [5], Robert Pietrasik [6], Jaroslav Mosnacek [2,7], Joanna Pietrasik* [1]

[1] Lodz University of Technology, Department of Chemistry, Institute of Polymer and Dye Technology, Stefanowskiego 12/16, 90 924 Lodz, Poland

[2] Polymer Institute, Slovak Academy of Sciences, Dubravska cesta 9, Bratislava 845 41, Slovakia

[3] Tomas Bata University in Zlin, University Institute, Centre of Polymer Systems, Trida T. Bati 5678, Zlin 76001, Czech Republic

[4] Institute of Macromolecular Chemistry, Czech Academy of Sciences, Heyrovskeho namesti 2, 162 06 Praha 6, Czech Republic

[5] Johannes Kepler University Linz, Institute of Polymer Sciences, Altenberger Str 69, A-4040 Linz, Austria

[6] Lodz University of Technology, Institute of Materials Science and Engineering, Stefanowskiego 1/15, 90 924 Lodz, Poland

[7] Centre for Advanced Material Application, Slovak Academy of Sciences, Dubravska cesta 9, 845 11 Bratislava, Slovakia

Synthesis of graphene oxide

The synthesis of graphene oxide was performed according to the modified Brodie method [1]. Fuming nitric acid (100 %, 125 mL) was added to a reaction flask containing a magnetic stirring bar. The mixture was subsequently cooled to approximately 0 °C in a water/ice bath and graphite (10 g) was loaded to the flask. The mixture was stirred to obtain a homogenous dispersion. Potassium chlorate (50 g) was slowly added to the blend while keeping the reaction at 0 °C. Upon complete dissolution of the potassium chlorate, the reaction flask was loosely capped to allow escape of the gas evolved and the mixture was stirred for 20 hours at 40 °C. After the end of the reaction, the mixture was added to 1L of deionized water (DW) and centrifuged, this was done three times. Then the GO was dispersed in 5 % HCl solution (3 L) to remove metal ions and centrifuged. Finally, it was cleaned by DW and dried in a freeze-drier. The surface area of GO was determined by BET analysis and was found to be 9.04 $m^2 g^{-1}$.

Synthesis of graphene oxide grafted bromo-2-methylpropionyl bromide (BiBB) ATRP initiator

The ATRP initiator bromo-2-methylpropionyl bromide (BiBB) was introduced onto the surface of graphene oxide *via* esterification according to the literature procedure [2]. The GO powder (2 g) was added to three-neck round-bottom flask (250 mL), then the flask was evacuated and back filled with argon several times. The THF (60 mL) was dried over sodium wires, freshly distilled and added to flask with GO under argon flow. The mixture was sonicated for a short time in an

ultrasound bath to disperse the particles in the solvent. Then the triethylamine (12mL, 86 mmol) was added into the reaction flask under argon flow. The mixture was cooled down to -5 °C in an ice/water bath and BiBB (7 mL, 57 mmol) was added dropwise. The reaction flask was sealed with septum and kept under inert atmosphere through balloon filled with the argon. The mixture was stirred at RT overnight (18 h), and then it was refluxed at 80 °C for one hour. The product was purified by filtration with a PTFE 0.44 μm membrane. The reaction mixture was filtered and washed with 100 mL acetone. Then it was dispersed in 200 mL DMF, briefly sonicated (30 s), filtered, and washed with acetone. This procedure was repeated three times (until the filtrate was clear). Finally, the product was washed with diethyl ether and dried in an oven at 60 °C for 12 h under vacuum. This procedure yielded the graphene oxide containing the initiator (GO-I).

Results and discussion

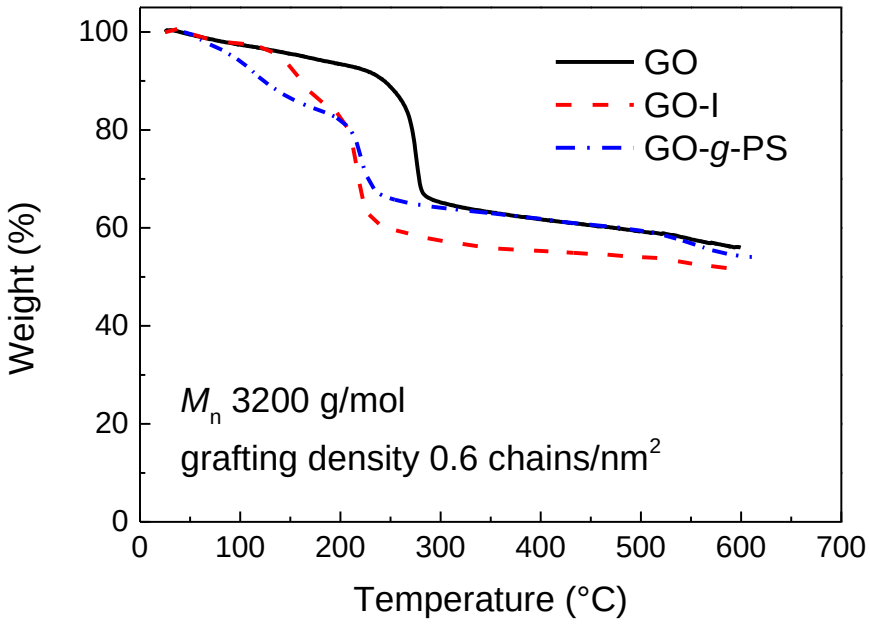

Fig. S1. Thermogravimetric analysis of neat GO, GO-I and GO-*g*-PS.

Grafting density (σ) is defined as the number of polymer chains per surface area (chain/nm^2). In this manuscript the value was estimated based on the commonly used approach using M_n values obtained from GPC, polymer content (PC, -) determined by TGA , and surface area determined by BET (SA, m^2/g) analysis and Avogadro constant (N_a, mol^{-1}) [3, 4]. The amount of polymer, M_n and Avogdro constant enables calculation of the amount of chains per 1 gram, and surface area enables calculation of the number of chains per area. The estimatation of grafting density can be then expressed by equation S1:

$$\sigma = \frac{PC}{M_n} \cdot \frac{N_a}{SA} \qquad \text{(S1).}$$

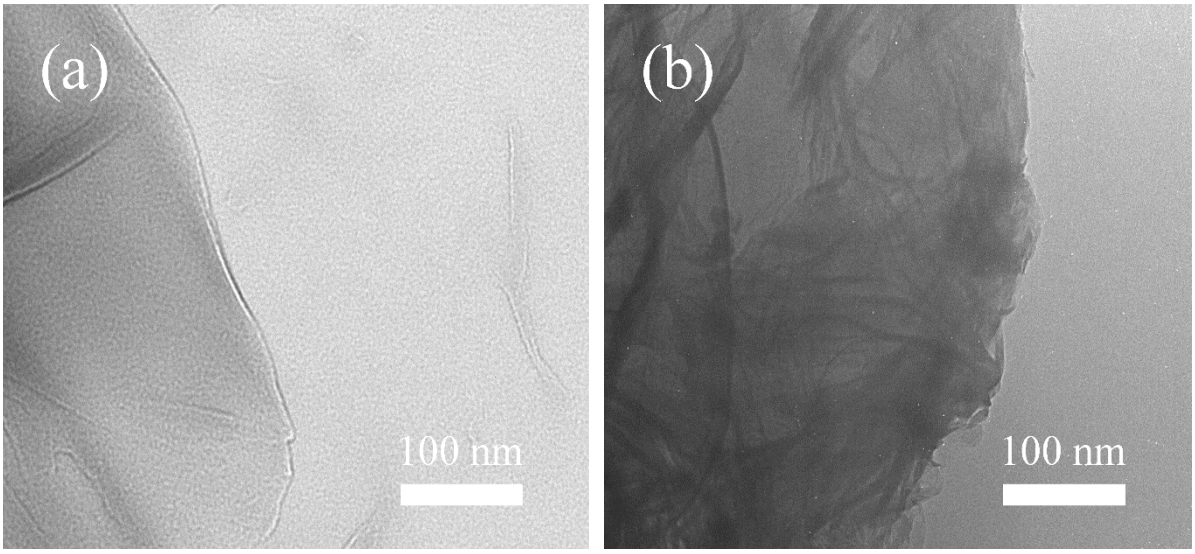

Fig. S2. TEM micrographs of GO (a) and GO-*g*-PS (b).

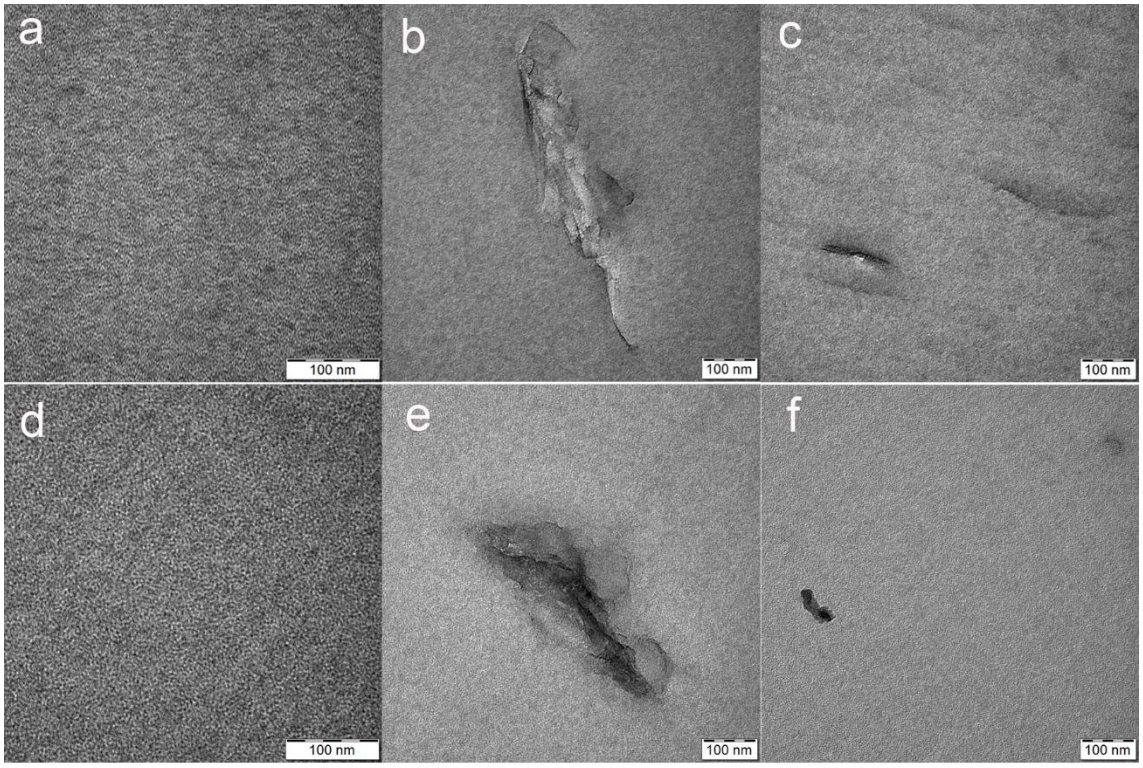

Fig. S3. TEM micrographs of PMMA/SAN blends with 40/60 (a, b, c) and 60/40 compositions (d, e, f) showing neat blends (a, d), composites enriched with neat GO (b, e), and composites enriched with GO-*g*-PS (c, f).

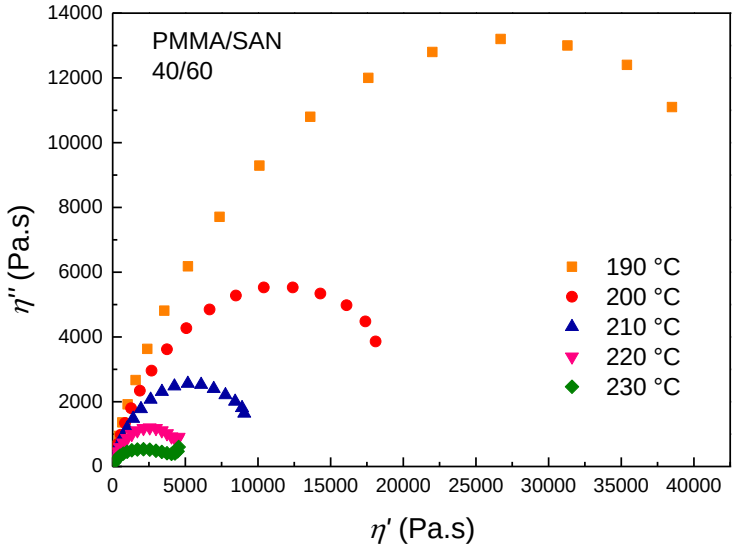

Fig. S4. Cole-Cole plot of PMMA/SAN 40/60 at various temperatures.

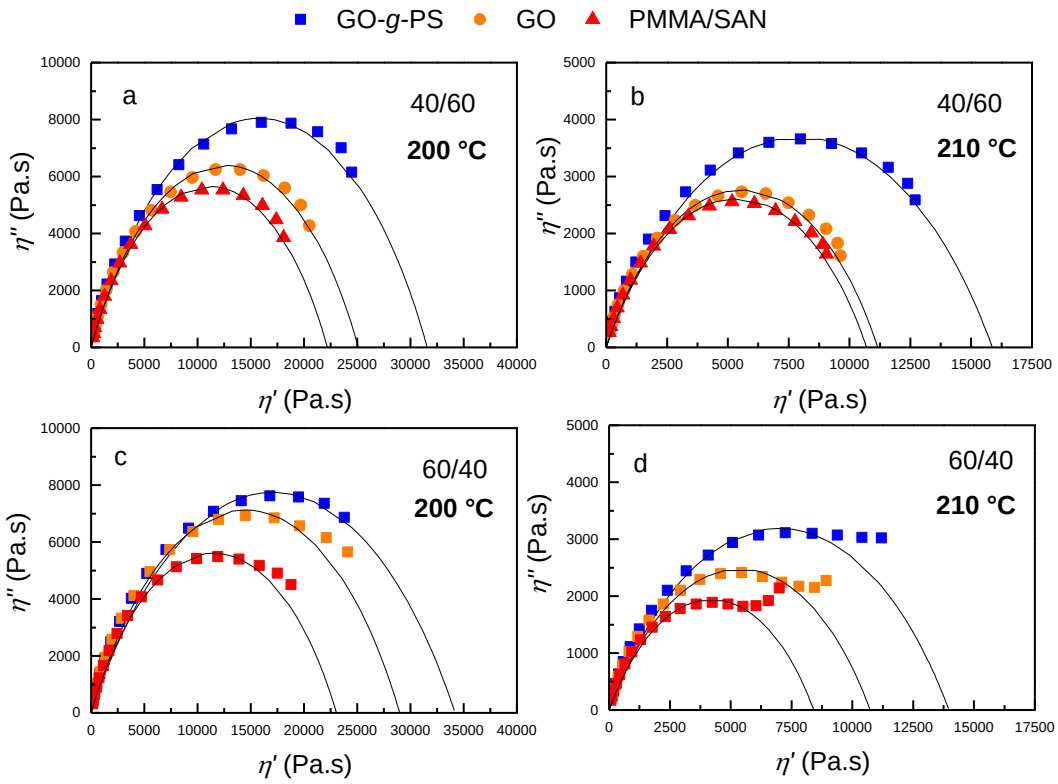

Fig. S5. Viscoelastic properties of 40/60 and 60/40 blends filled by neat GO and GO-*g*-PS at 200 °C and 210 °C. The data in Cole-Cole representation fit with Cole-Cole model.

The wetting coeficient calculations

It was not possible to predict the GO location in PMMA/SAN blend at higher temperatures (190°C - 220°C) because, as far we know, there are no available data about the temperature coefficient. Since the estimated grafting density of PS on GO surface is high (0.6 chains nm^{-2}) it could be assumed that that the interaction of GO-g-PS with PMMA/SAN matrices are provided only by the accessible PS brushes. For that reason, GO was not included in the calculations. The interfacial tensions were calculated using harmonic mean equations [5] (surface tension γ of PMMA, SAN an PS, and its dispersive γ^d and polar γ^p components taken for interfacial tensions γ_{12} calculations

are presented under Table S1). At all studied temperatures, from 180 °C to 220 °C, the wetting parameter for PMMA/SAN/PS equals $\omega = 0.68$, suggesting that when PS is tethered to GO surface the obtained GO-*g*-PS hybrids are located at the interphase of PMMA and SAN. However, the theoretical predictions do not take into account the change of polymer polarity with temperature and the impact of the molecular weight of polymers on the surface tension.

Table S1 Calculated interfacial tensions γ_{12} and wetting parameters ω at varied temperatures T; from 180 °C to 220 °C.

T [°C]	γ_{12} [mN m^{-1}]*			ω
	PS/PMMA	PS/SAN	PMMA/SAN	PMMA/SAN/PS
190	0.98	4.65	5.41	0.68
200	0.96	4.53	5.27	0.68
210	0.93	4.42	5.13	0.68
220	0.91	4.30	4.99	0.68

**Data used for γ calculations of polymer surface tension at given temperature; PS: γ = 40.7- 0.072(T-20), γ^p/γ =0.17 [6]; PMMA: γ = 41.1- 0.076(T-20); γ^p/γ =0.28 [6];SAN: γ = 41.5- 0.07(T-20, γ^p/γ =0.15)[7]*

Dielectric spectroscopy

In the Fig. S6a the dielectric map of PMMA is shown. The relaxation of methyl groups bonded to the main chain of PMMA (γ relaxation) was observed at temperatures from – 140 °C to – 60 °C as a small peak. The relaxation in the temperature range from -20 °C to 100 °C is attributed to the partial rotation of the CH_3COOCH_3 around the C-C bond linking the side groups to the main chain of PMMA (β relaxation). Above T_g, both α and the β processes relax, with increasing temperature they split to appear as $\alpha\beta$ cooperative relaxation [8-10]. Moreover, due to presence of both relaxations α and the β above the T_g, it is difficult to fit the α relaxation in the measured frequency

range [9] and therefore the $\alpha\beta$ relaxation was evaluated from the point of view of activation energy similarly as was done by Soreto et. al. [11]. At high temperatures and low frequencies, the MWS polarization is clearly visible. This polarization appears at the interfaces of components with different relative permittivities and/ or electrical conductivities, then the charge remains blocked at the interface that manifest itself as a polarization peak [12, 13]. In the dielectric map of SAN, Fig. S6b, the relaxation of acrylonitrile side group (γ) from SAN appears in the temperature range from – 150 °C to -50 °C as a small peak. Above T_g, α transition of SAN and also MWS at high temperature and low frequencies can be seen. Here, all relaxation processes are well-distinguishable especially α transition in comparison to neat PMMA.

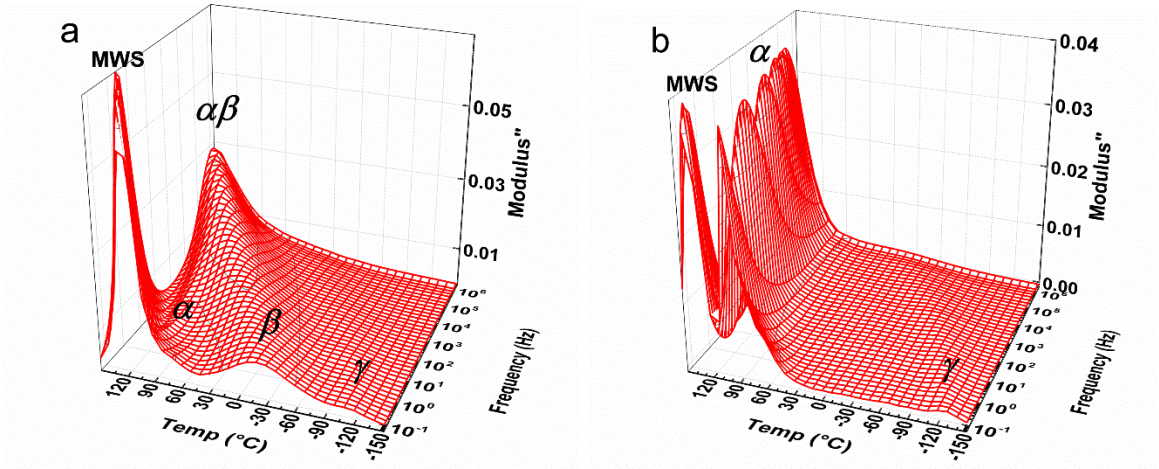

Fig. S6. Dielectric relaxation map of PMMA (a) and SAN (b)

In the Fig. 7Sa and Fig. 7Sb the temperature dependence of 40/60 and 60/40 PMMA/SAN blend systems are shown, respectively. The spectra collected at low frequency, 10 Hz, were plotted to clearly observe all relaxations. The results are depicted in dielectric loss modulus (*M''*)

representation to avoid the contribution of electrode polarization, that appears at low frequency and high temperatures and usually overlap MWS polarization [14].

In the both types of blends 40/60 and 60/40, the γ relaxations of PMMA and SAN are overlapped completely in the whole investigated temperature and frequency range, Fig. S8a and Fig. S8b, respectively, therefore they were omitted in further discussion, since the effect of the compatibilizer addition is hardly distinguishable. The β relaxation of PMMA was clearly visible in case of both blends. The SAN α relaxation appeared from 110 °C to 150 °C. It overlaps with PMMA α relaxation at low frequencies and PMMA $\alpha\beta$ relaxation at higher frequencies. However, in frequency dependencies measured over the temperature range from 110 °C to 130 °C the peak maxima of both PMMA and SAN were able to be distinguished enabling the filler effects to be followed, Fig. S7.

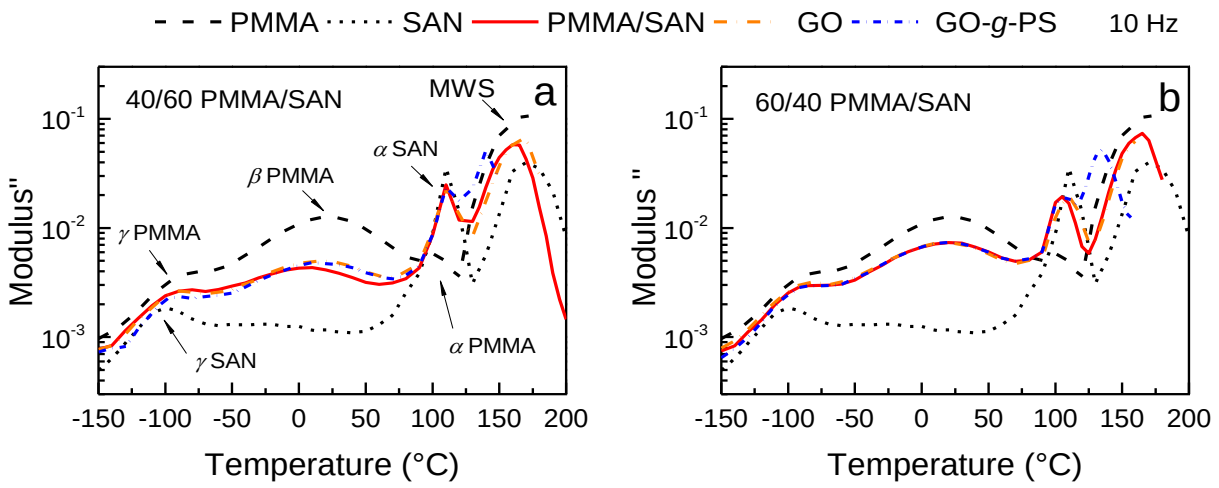

Fig. S7. Temperature dependence of PMMA/SAN blends at measured 10 Hz a) 40/60 blend system, b) 60/40 blend system

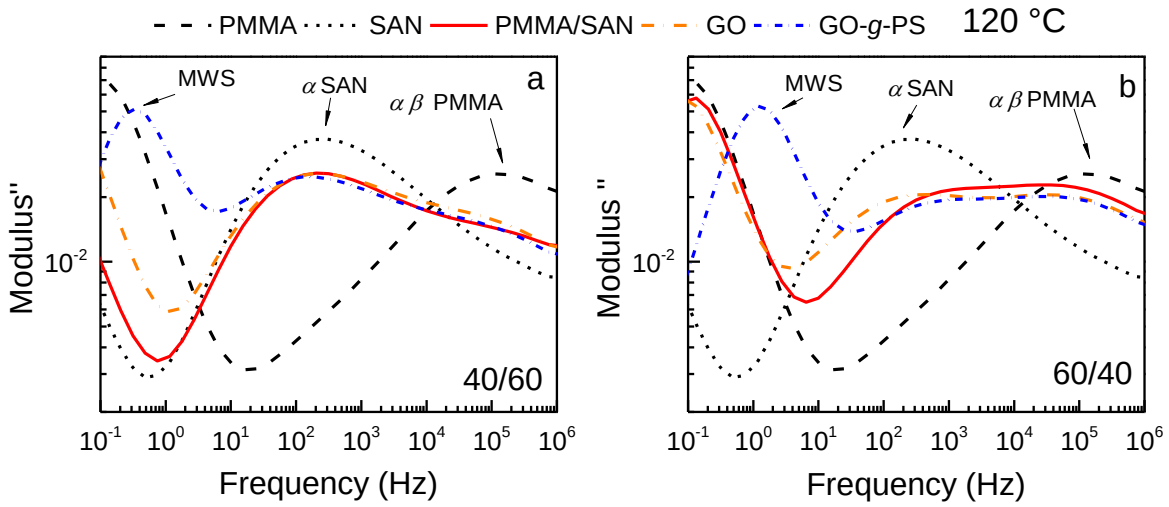

Fig. S8. Frequency dependence of dielectric loss modulus of PMMA/SAN blends measured at 130 °C a) 40/60 and b) 60/40

Table S2 Activation energies of CN and CH_3 based on Arrhenius

Sample	SAN γ relaxation of CN	PMMA γ relaxation of CH_3
	E_a (kJ mol^{-1})	E_a (kJ mol^{-1})
PMMA	x	16.8
SAN	17.1	x
PMMA/SAN 40/60	17.1	16.8
PMMA/SAN 60/40	17.1	16.8
PMMA/SAN 40/60 GO	17.2	16.9
PMMA/SAN 60/40 GO	17.2	16.9
PMMA/SAN 40/60 GO-*g*-PS	17.2	16.9
PMMA/SAN 60/40 GO-*g*-PS	17.2	16.9

Table S3 Parameters of VFT fits of PMMA $\alpha\beta$ relaxation and SAN α relaxations, and Arrhenius fit of PMMA β relaxation

	aβ-relaxation PMMA			VFT *α*-relaxation SAN			*β*-relaxation PMMA O-CH_3	
PMMA/SAN	log f_0 (s^{-1})	T_0 (K)	E_a (kJ mol^{-1})	log f_0 (s^{-1})	T_0 (K)	E_a (kJ mol^{-1})	log f_0 (s^{-1})	E_a (kJ mol^{-1})
40/60	-10.7	290	65.6	-10.1	341	63.0	-14.4	27.7
40/60 GO	-10.9	298	68.9	-10.1	342	63.9	-15.2	28.6
40/60 GO-*g*-PS	-11.2	305	72.1	-10.2	345	65.1	-15.4	28.7
60/40	-11.0	300	66.3	-10.3	343	64.2	-15.8	29.9
60/40 GO	-11.4	310	75.2	-10.4	345	65.5	-16.1	30.3
60/40 GO-*g*-PS	-11.8	318	82.7	-10.5	348	66.3	-16.4	30.4

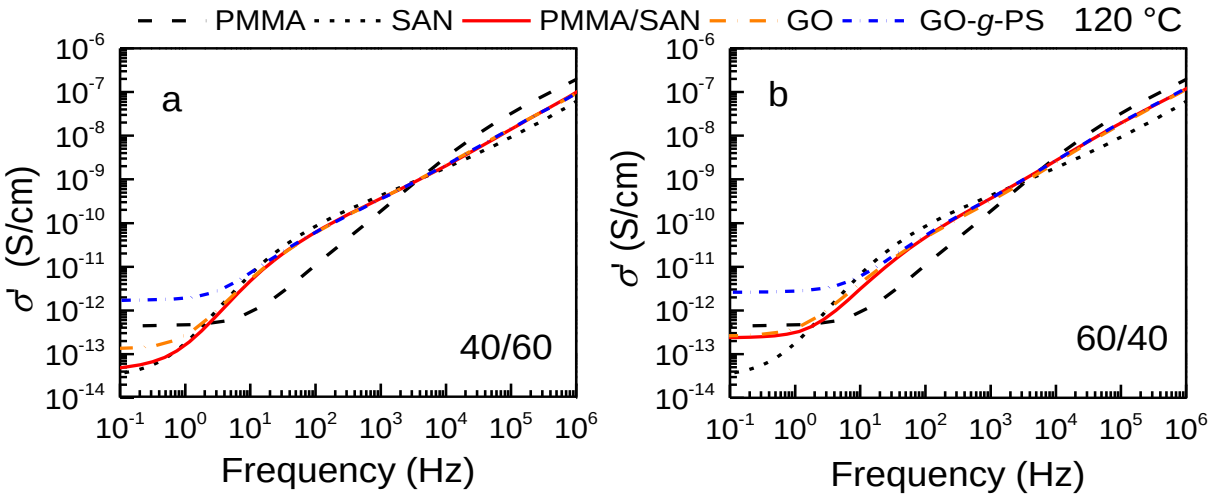

Fig. S9. Frequency dependence of electrical conductivity of 40/60 (a) and 60/40 (b) blend system at 120 °C

Literature

[1] O. Jankovsky, P. Marvan, M. Novacek, J. Luxa, V. Mazanek, K. Klimova, D. Sedmidubsky, Z. Sofer, Synthesis procedure and type of graphite oxide strongly influence resulting graphene properties, Applied Materials Today 4 (2016) 45-53.

[2] M. Ilcikova, M. Mrlik, Z. Spitalsky, M. Micusik, K. Csomorova, V. Sasinkova, A. Kleinova, J. Mosnacek, A tertiary amine in two competitive processes: reduction of graphene oxide vs. catalysis of atom transfer radical polymerization, Rsc Advances 5(5) (2015) 3370-3376.

[3] A. Dang, S. Ojha, C.M. Hui, C. Mahoney, K. Matyjaszewski, M.R. Bockstaller, High-Transparency Polymer Nanocomposites Enabled by Polymer-Graft Modification of Particle Fillers, Langmuir 30(48) (2014) 14434-14442.

[4] Z.Y. Wang, C. Mahoney, J.J. Yan, Z. Lu, R. Ferebee, D.L. Luo, M.R. Bockstaller, K. Matyjaszewski, Preparation of Well-Defined Poly(styrene-co-acrylonitrile)/ZnO Hybrid Nanoparticles by an Efficient Ligand Exchange Strategy, Langmuir 32(49) (2016) 13207-13213.

[5] S. Wu, Calculation of interfacial tension in polymer systems, Journal of Polymer Science Part C-Polymer Symposium (34) (1971) 19-&.

[6] S. Wu, Interfacial and surface tension in polymers, J. Macromol. Sci.-Rev. Macromol. Chem. Phys. C 10(1) (1974) 1-73.

[7] E.N. Ito, M.M. Ueki, R.E.S. Bretas, E. Hage, Interfacial Tension of PBT/SAN Blends by the Drop Retraction Method, Mater. Res.-Ibero-am. J. Mater. 11(2) (2008) 165-169.

[8] R. Bergman, F. Alvarez, A. Alegria, J. Colmenero, The merging of the dielectric alpha- and beta-relaxations in poly(methyl methacrylate), J. Chem. Phys. 109(17) (1998) 7546-7555.

[9] S. Hirota, Y. Tominaga, S. Asai, M. Sumita, Dielectric relaxation behavior of poly(methyl methacrylate) under high-pressure carbon dioxide, J. Polym. Sci. Pt. B-Polym. Phys. 43(21) (2005) 2951-2962.

[10] F. Garwe, A. Schonhals, H. Lockwenz, M. Beiner, K. Schroter, E. Donth, Influence of cooperative alpha dynamics on local beta relaxation during the development of the dynamic glass transition in poly(n-alkyl methacrylate)s, Macromolecules 29(1) (1996) 247-253.

[11] S.S. Teixeira, C.J. Dias, M. Dionisio, L.C. Costa, New method to analyze dielectric relaxation processes: a study on polymethacrylate series, Polym. Int. 62(12) (2013) 1744-1749.

[12] F.K.a.A. Schonhals, Broadband dielectric Specroscopy, Springer-Verlag Berlin Heidelberg2003.

[13] A. Bharati, M. Wubbenhorst, P. Moldenaers, R. Cardinaels, Effect of Compatibilization on Interfacial Polarization and Intrinsic Length Scales in Biphasic Polymer Blends of P alpha MSAN and PMMA: A Combined Experimental and Modeling Dielectric Study, Macromolecules 49(4) (2016) 1464-1478.

[14] M. Mrlik, R. Moucka, M. Ilcikova, P. Bober, N. Kazantseva, Z. Spitalsky, M. Trchova, J. Stejskal, Charge transport and dielectric relaxation processes in aniline-based oligomers, Synth. Met. 192 (2014) 37-42.